9-13-2018

Phononic rogue waves

E. G. Charalampidis
University of Massachusetts Amherst

J. Lee
University of Massachusetts Amherst

P. G. Kevrekidis
University of Massachusetts Amherst

C. Chong
Bowdoin College

Phononic rogue waves

E. G. Charalampidis, J. Lee, and P. G. Kevrekidis
Department of Mathematics and Statistics, University of Massachusetts Amherst, Amherst, Massachusetts 01003-4515, USA

C. Chong*
Department of Mathematics, Bowdoin College, Brunswick, Maine 04011, USA

(Received 17 January 2018; revised manuscript received 2 July 2018; published 13 September 2018)

We present a theoretical study of extreme events occurring in phononic lattices. In particular, we focus on the formation of rogue or freak waves, which are characterized by their localization in both spatial and temporal domains. We consider two examples. The first one is the prototypical nonlinear mass-spring system in the form of a homogeneous Fermi-Pasta-Ulam-Tsingou (FPUT) lattice with a polynomial potential. By deriving an approximation based on the nonlinear Schrödinger (NLS) equation, we are able to initialize the FPUT model using a suitably transformed Peregrine soliton solution of the NLS equation, obtaining dynamics that resembles a rogue wave on the FPUT lattice. We also show that Gaussian initial data can lead to dynamics featuring a rogue wave for sufficiently wide Gaussians. The second example is a diatomic granular crystal exhibiting rogue-wave-like dynamics, which we also obtain through an NLS reduction and numerical simulations. The granular crystal (a chain of particles that interact elastically) is a widely studied system that lends itself to experimental studies. This study serves to illustrate the potential of such dynamical lattices towards the experimental observation of acoustic rogue waves.

DOI: 10.1103/PhysRevE.98.032903

I. INTRODUCTION

Extreme wave events, such as freak or rogue waves, are waves that seem to appear out of nowhere, and then vanish without a trace [1–3]. The term rogue wave was first coined to describe an ocean wave that has an amplitude greater than twice the significant wave height [1]. Based on the classical description of waves that assumes a Rayleigh distribution of wave heights, a rogue wave should be an extremely rare event [1]. The measurement of an ocean rogue wave (the Draupner wave) in 1995 initiated an intense interest in the subject of extreme events. It has been found that ocean rogue waves occur more regularly than the statistical description predicts [1], and a number of alternative mechanisms for the formation of rogue waves has been produced [1]. One such approach is through the derivation of simple modulation equations such as the nonlinear Schrödinger (NLS) equation from the underlying equations of motion [4]. The Peregrine soliton solution of the focusing NLS equation sits atop a finite background, and is localized in both space and time [5]. The maximum amplitude of the Peregrine soliton is three times greater than the background upon which it sits and is therefore a prominent rogue wave candidate. Such structures have been studied in various media, including nonlinear optics [6–10], mode-locked lasers [11], superfluid helium [12], hydrodynamics [13–15], Faraday surface ripples [16], parametrically driven capillary waves [17], plasmas [18], ultracold gases [19], and electrical transmission lines [20]. A unifying theme of these varied physical settings of rogue waves is the relevance of the NLS setting as an approximate model equation. Rogue waves in discrete systems are far less studied. One example of such a study concerns rogue waves in the integrable Ablowitz-Ladik lattice [21], which is known to have an exact solution that has similar properties as the NLS Peregrine soliton. At the level of granular systems, the pioneering work of Ref. [22] was, to the best of our knowledge, the first to recognize the potential of such systems for unusually large (rogue) fluctuations in late-time dynamics, in the absence of dissipation.

The present study concerns a different (than those of NLS type) discrete system, namely, phononic lattices, which are systems that manipulate pressure waves (as opposed to photonic latices in which light waves are manipulated). Arguably, one of the most prototypical phononic lattices is the Fermi-Pasta-Ulam-Tsingou (FPUT) lattice, which describes an one-dimensional system of masses coupled through weakly nonlinear springs [23]. While the amount of research efforts in the direction of the FPUT lattice is immense (see the book [24] but also the recent review [25]), rogue waves in FPUT lattices have not been reported on, to the best of our knowledge. In the small amplitude limit, the NLS equation is once again a valid modulation equation, suggesting that extreme events are possible to observe in phononic lattices. At the same time, we must also recognize that there are limits to the descriptive power of the NLS equation (failing, e.g., for larger amplitude excitations). Thus, we will also employ numerical simulations to explore the possibility of extreme events in phononic systems, as well as to monitor the by-products of the nonintegrability and deviations from the NLS of the full granular setting. The conclusion of these studies will be that while such deviation features will be markedly present, so will be the space-time localization of the Peregrine solitons (and generalizations thereof), suggesting the relevance of such systems for manifesting this phenomenology.

*cchong@bowdoin.edu

To demonstrate that a phononic rogue wave could in principle be observed experimentally, we conduct a study in the case of an one-dimensional chain of beads interacting through Hertzian contacts, i.e., a granular crystal. Over the last two decades, granular crystals have received considerable attention, as is now summarized in a wide range of reviews [26–33]. Granular crystals are remarkably tunable, which permits one to access weakly or strongly nonlinear dynamic responses. At the same time, it is possible to easily access and arrange the media in a wide range of configurations (homogeneous, periodic, chains with impurities, chains with local resonators, disordered chains, and many others). These aspects make the study of granular crystals fascinating from both fundamental and applied perspectives [31].

The remainder of the paper is structured as follows. In Sec. II, we examine a homogeneous FPUT lattice. We derive a focusing NLS equation, which describes the modulation of small amplitude and rapidly oscillating plane waves in time and space. The Peregrine soliton of the NLS equation is used to initialize the FPUT system, which leads to rogue-wave-like dynamics. The prediction based on the NLS approximation coincides with the numerical simulations of the FPUT lattice up until the formation of the large amplitude wave. While the NLS approximation sees a decreasing and "vanishing" of the large amplitude wave back towards the background, the presence of a modulational instability causes the formation of outward propagating waves from the center of the lattice. We also explore generalized pulselike initial data (in the form of Gaussian wave packets), which can lead to a wide variety of behaviors including soliton dynamics, breathing dynamics, and rogue wave dynamics. The amplitude of the initial conditions "selects" the type of observed dynamics. In Sec. III we consider a diatomic granular crystal lattice. Using a focusing NLS equation derived as an envelope approximation of this diatomic chain, we once again use the Peregrine soliton solution of the NLS equation to initialize the lattice dynamics. We find qualitatively similar behavior to that reported for the homogeneous FPUT lattice for all mass ratios tested. A noteworthy finding is that the sensitivity to boundary effects appears to depend on the chosen mass ratio. Section IV draws conclusions and discusses future directions.

II. HOMOGENEOUS FERMI-PASTA-ULAM-TSINGOU LATTICES

A. Theoretical setup

The prototypical Fermi-Pasta-Ulam-Tsingou (FPUT) lattice has the form

$$\ddot{u}_n = V'(u_{n+1} - u_n) - V'(u_n - u_{n-1}) \tag{1}$$

with

$$V'(x) = K_2 x + K_3 x^2 + K_4 x^3, \tag{2}$$

where $n \in I$, with I a countable index set, and $u_n = u_n(t) \in \mathbb{R}$ is the displacement of the nth particle from equilibrium position at time t. Equation (1) with $I = \mathbb{Z}$ has the Hamiltonian

$$H = \sum_{n\in\mathbb{Z}} \frac{1}{2}\dot{u}_n^2 + V(u_{n+1} - u_n).$$

The linear problem (i.e., when $K_3 = K_4 = 0$) is solved by

$$u_n(t) = e^{i(kn+\ t)}$$

for all $k \in [0, \pi]$, where and k are related through the dispersion relation,

$$(k)^2 = 4K_2 \sin^2(k/2),$$

such that the cutoff point of the acoustic band is $2\sqrt{K_2}$; see Fig. 1(a). Motivated by prior works on rogue waves where the Peregrine soliton is used to describe the formation of such structures, we first derive the NLS equation from Eq. (1). When deriving the NLS equation as a modulation equation, one uses the multiple scale ansatz

$$u_n(t) \approx \psi_n(t) := \varepsilon\{B(X,T) + [A(X,T)E + \text{c.c.}]\},$$
$$E = e^{i(k_0 n + \ _0 t)}, \quad X = \varepsilon(n + ct), \quad T = \varepsilon^2 t, \tag{3}$$

where $\varepsilon \ll 1$ is a small parameter, effectively parametrizing the solution amplitude (and also its inverse width). Directly substituting this ansatz into Eq. (1) and equating the various orders of ε leads to the dispersion relation $_0 = (k_0)$ at $O(\varepsilon)$, the group velocity relation $c = \ '(k_0)$ at $O(\varepsilon^2)$, and the nonlinear Schrödinger equation

$$i\,\partial_T A(X,T) + \nu_2 \partial_X^2 A(X,T) + \nu_3 A(X,T)|A(X,T)|^2 = 0 \tag{4}$$

at $O(\varepsilon^3)$, where $\nu_2 = -\ ''(k_0)/2 > 0$ and ν_3 is a lengthy wave-number-dependent expression. Full details of the derivation of the NLS equation starting from Eq. (1), including the higher-order terms of the ansatz, can be found, e.g., in Refs. [34–36]. Since we seek standing wave solutions, we choose the wave number to be at the edge of the acoustic band $k_0 = \pi$, such that the group velocity vanishes, $_0 = 2\sqrt{K_2}$, and

$$\nu_3|_{k_0=\pi} = \frac{4}{K_2\sqrt{K_2}}(3K_2K_4 - 4K_3^2) = b.$$

Since $\nu_2 > 0$, the NLS equation (4) will be focusing if $b > 0$. For our numerical computations, we consider the case example of $K_2 = K_4 = 1$ and $K_3 = 1/\sqrt{2}$ such that $\nu_2 = 1/4$ and $b = 4$. The equation for $B(X,T)$ is defined in terms of $A(X,T)$,

$$\partial_X B(X,T) = \frac{4K_3[1 - \cos(k)]}{[\ '(k)]^2 - [\ '(0)]^2}|A(X,T)|^2. \tag{5}$$

B. Peregrine initial data

The focusing NLS equation has the one-parameter family of Peregrine soliton solutions [37] given by

$$A(X,T) = \sqrt{\frac{P_0}{\nu_3}}\left[1 - \frac{4(1 + 2P_0\, iT)}{1 + \frac{2}{\nu_2}P_0X^2 + 4P_0^2T^2}\right]e^{iP_0T}, \tag{6}$$

where $P_0 > 0$ is an arbitrary parameter. This solution is localized in space and time and has a maximum [located at $(X,T) = (0,0)$] that is three times greater than its background, which are the features we desire to describe a rogue wave; see Fig. 1(b). Using the Peregrine soliton for the envelope function and a wave number $k_0 = \pi$, $K_2 = K_4 = 1$ and $K_3 = 1/\sqrt{2}$ we

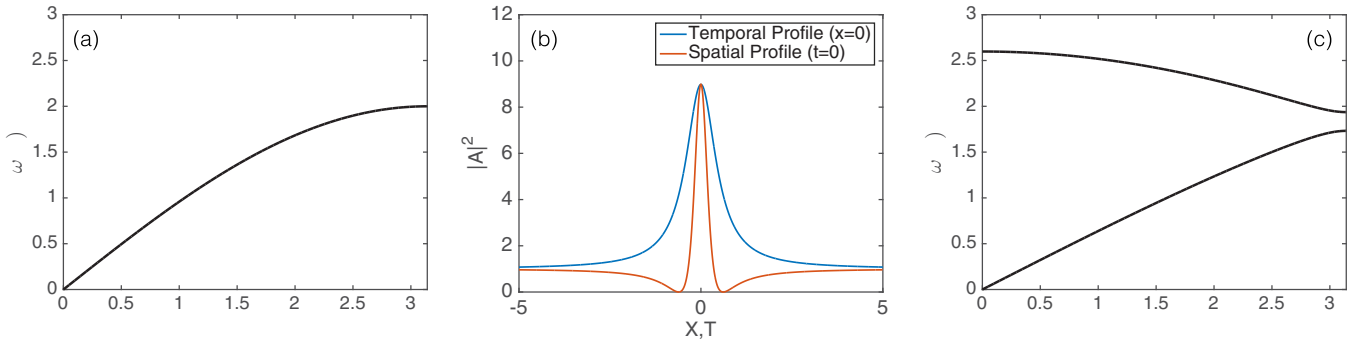

FIG. 1. (a) Dispersion relation for the monomer FPUT lattice with $K_2 = 1$, which consists of an acoustic branch only. (b) The spatial profile of the Peregrine soliton at $T = 0$ and the temporal profile at $X = 0$. (c) Dispersion relation for the dimer FPUT lattice with $K_2 = 3/2$ and $\rho = 0.8$, which consists of an acoustic branch (lower branch) and optical branch (upper branch).

arrive at the following approximation:

$$u_n(t) = \frac{\sqrt{\eta}}{2}\left[1 - \frac{4(1+2i\eta t)}{1+8\eta n^2+4(\eta t)^2}\right]e^{i(\pi n+(2+\eta)t)} + \text{c.c.} + \varepsilon B(\varepsilon n, \varepsilon^2 t), \quad \eta = P_0\varepsilon^2, \tag{7}$$

where B is defined in Eq. (5). It will be convenient to represent the solution in the strain variable formulation, that is, $y_n = u_{n+1} - u_n$ since the term B in the ansatz, which introduces a linear slope, will vanish. The parameter $\eta = P_0\varepsilon^2 > 0$ selects the background amplitude [since $|y_n(0)|$ $2\sqrt{\eta}$ as n $\pm\infty$] and the frequency of oscillation $2+\eta$, which lies above the cutoff of the acoustic band $_0 = 2$.

To test the validity of the multiscale analysis, we perform numerical simulations of the FPUT model Eq. (1) using Eq. (7) as initial data. For instance, see Fig. 2 for a simulation with $\varepsilon = 0.02$, $X \in [-40, 40]$ and $T \in [-5, 5]$. In this simulation, our initial time is $t = -5\varepsilon^2$, such that $t = 0$ should correspond to a peak at the middle node $n = 0$. The simulations are sensitive to the boundary conditions since the background is nonzero (we employ boundary conditions that are periodic in the strain). Therefore, we take a larger spatial domain to reduce the influence of the boundary, since we are mainly concerned with the core of the solution. For times before the rogue wave appears (i.e., $t < 0$) the FPUT dynamics is predicted by the NLS dynamics [compare Fig. 2(a) and 2(b)]. After the formation of the rogue wave, i.e., for $t > 0$, the FPUT dynamics departs from the NLS prediction. In the FPUT case, the large amplitude portion of the wave breaks into smaller, but still large relative to the background, waves. We believe that the emergence of these waves stemming from the Peregrine soliton core is a by-product of the modulational instability of the NLS background as transcribed into the FPUT lattice and as seeded by the large amplitude perturbation induced by the wave structure.

C. Gaussian initial data

It has been shown through the rigorous work of Ref. [38] that Peregrine-like structures are a generic by-product of the so-called gradient catastrophe phenomenon that the (focusing) NLS is subject to for localized initial data in the semiclassical limit. This feature has led also to very clean recent observations of Peregrine solitons in optical systems [39]. Also, at a numerical level, systematic explorations of Gaussian initial data have led to roguelike waves in the focusing NLS equation for sufficiently broad Gaussians [19]. When sufficiently broad (so as to be rescalable to the semiclassical regime), the waves evolving through the equations of motion focus their energy to the center in a Peregrine structure. Even more remarkably, such initial data subsequently lead to the formation of an array of essentially identical (up to small corrections) Peregrine-like

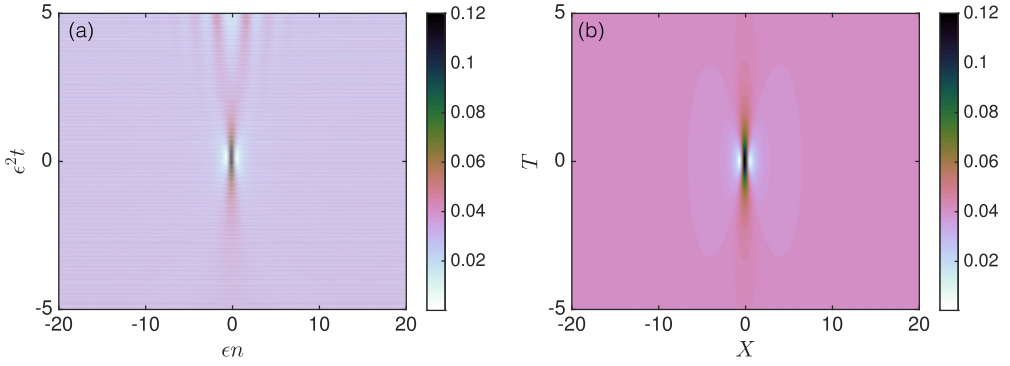

FIG. 2. (a) Simulation of Eq. (1) with $\varepsilon = 0.02$, $X \in [-40, 40]$ and $T \in [-5, 5]$ that is initialized with Eq. (7) and $P_0 = 1$. Color intensity corresponds to the strain $|y_n(t)|$. Notice that the space-time evolution here and in the figures that follow is given in terms of the rescaled variables εn and $\varepsilon^2 t$ for space and time, respectively. (b) Corresponding NLS prediction $2\varepsilon|A(X, T)|$. Note that the background amplitude of $|y_n(t_0)|$ is the same as $2\varepsilon|A(X, T_0)|$.

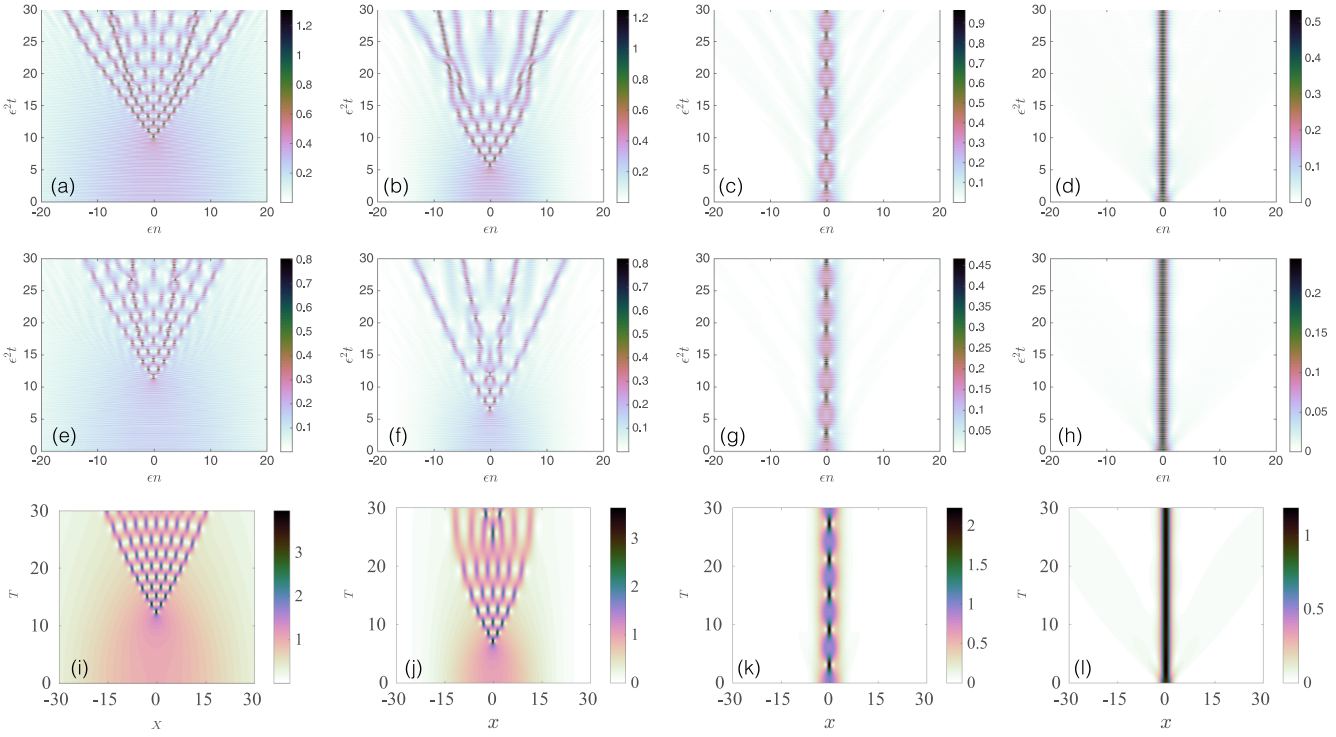

FIG. 3. Simulation of Eq. (1) that is initialized with Eq. (3) with A given by Eq. (8) with the following width parameters $\sigma = 20.1$ for panels (a, e, i), $\sigma = 10.5$ for panels (b, f, j), $\sigma = 2.5$ for panels (c, g, k) and $\sigma = 1.3$ for panels (d, h, l). In panels (a)–(d) the perturbation parameter value is $\varepsilon = 0.1$. In panels (e)–(h) the perturbation parameter value is $\varepsilon = 0.05$. Panels (i)–(l) correspond to the respective numerical simulations of the NLS equation with Gaussian initial data; see, e.g., Ref. [19].

structures, arising at the poles of the so-called tritronquee solution of the Painlevé I equation.

On the other hand, if the Gaussian is sufficiently narrow, then a solution more akin to a soliton forms; see the top panel of Fig. 3 for a few examples. Here we investigate if a similar phenomenology is possible in the FPUT lattice. More specifically, we consider initial data for the envelope function $A(X, T)$ of the form

$$A(X, T = 0) := A_G(X) = \exp\left(\frac{-X^2}{4\sigma^2}\right). \tag{8}$$

In Fig. 3 results for simulations for the parameter values $\sigma \in \{20.1, 10.5, 2.5, 1.3\}$ for $\varepsilon = 0.1$ and $\varepsilon = 0.05$ are shown. Note the strong resemblance to the NLS prediction; however, after the main peak forms, there is noticeable distortion between the NLS prediction and the actual FPUT dynamics, just as the case in the Peregrine example in the previous subsection. In this simulation the tails are decaying to zero, and thus any potential boundary effects should be minimal. These findings confirm once again the genericity of the gradient catastrophe scenario of Ref. [38], although presumably the nonintegrability of the present lattice distorts the "Christmas-tree" pattern of the subsequent Peregrines in comparison to the NLS paradigm. Nevertheless, the pattern is still clearly discernible and progressively reverts to breathing and ultimately to solitonic solutions as σ decreases (i.e., along the horizontal direction). On the other hand, the trend of decreasing ε (along the vertical direction) makes the patterns appear more and more "NLS-like" as is expected by the increased accuracy of the NLS approximation in the limit of small ε.

III. DIATOMIC GRANULAR CRYSTAL

A. Theoretical setup

We now turn our attention to another variant of the FPUT model that considers a so-called Hertzian contact [26,27] for the nonlinearity rather than the polynomial nonlinearity considered in Eq. (1). Such a nonlinearity is relevant in the description of granular crystals when considering only forces due to elastic compression between the particles. In this case, the model equations are

$$\ddot{u}_n = \frac{A_n}{m_n}[\delta_{0,n} + u_{n-1} - u_n]_+^p - \frac{A_{n+1}}{m_n}[\delta_{0,n+1} + u_n - u_{n+1}]_+^p, \tag{9}$$

where u_n is the displacement of the nth particle measured from its equilibrium position in an initially compressed chain, m_n is the mass of the nth particle, and $\delta_n = (F_0/A_n)^{1/p}$ is a static displacement for each particle that arises from the static load $F_0 = \text{const}$. For spherical particles, the exponent is $p = 3/2$, and the parameter A_n, which reflects the material and the geometry of the chain's particles, has the form

$$A_n = \frac{4E_nE_{n+1}\sqrt{\frac{R_nR_{n+1}}{(R_n+R_{n+1})}}}{3E_{n+1}\left(1-\nu_n^2\right) + 3E_n\left(1-\nu_{n+1}^2\right)}, \tag{10}$$

where E_n is the elastic (Young) modulus of the nth particle, ν_n is its Poisson ratio, and R_n is its radius. Important special cases of Eq. (9) include monoatomic (i.e., "monomer") chains (in which all particles are identical, so $A_n = A$, $m_n = m$,

and $\delta_{0,n} = \delta_0$), period-2 diatomic chains, and chains with impurities (e.g., a "host" monomer chain with a small number of "defect" particles of a different type). In a monomer chain with strong precompression, Eq. (9) is well approximated by the FPUT model (1). To see this, let $V'(x) = -F(-x)$, and Taylor expand the nonlinearity $F(x) = [\delta_0 + x]_+^{3/2}$ about $x = 0$. This leads to

$$V'(x) = -\delta_0^{3/2} + K_2 x + K_3 x^2 + K_4 x^3, \quad K_2 = \frac{3}{2}\delta_0^{1/2},$$
$$K_3 = -\frac{3}{8}\delta_0^{-1/2}, \quad K_4 = -\frac{3}{48}\delta_0^{-3/2}. \tag{11}$$

Thus, in the small amplitude limit (where the above Taylor expansion is valid), one can apply the same multiple scale analysis as in Sec. II. However, in the case of the coefficients given in (11) the linear and nonlinear coefficients of the NLS equation are, respectively, $\nu_2 = -\ ''(\pi)/2 > 0$ and $\nu_3 = (K_2K_4 - 4K_3^2)/(K_2\sqrt{K_2}) < 0$, and thus, the relevant NLS equation for the monomer granular crystal is the defocusing NLS. While this case is interesting in its own right (allowing the existence of NLS dark solitons, and hence dark breathers of the granular crystal [40,41]), there are no Peregrine solitons. To obtain a focusing NLS equation (and hence the possibility of Peregrine solitons) we modify our lattice model such that there are additional branches in the dispersion. In particular, we seek a dispersion relation such that one branch has the opposite concavity of the acoustic branch of the monomer chain at $k = \pi$, namely, that $-\ ''(\pi)/2 < 0$. Such is the case for the dimer granular crystal [see Fig. 1(c)], which consists of alternating particles of two types, so $A_n = A$, $\delta_{0,n} = \delta_0$, and the mass is $m_n = m$ for even n and $m_n = M$ for odd n. In such a chain, the mass ratio $\rho = m/M$ is the only additional parameter beyond the monomer case. If we introduce new variables v_n to represent the displacement of the even particles (e.g., $v_n = u_{2k}$) and w_n to represent the displacement of the odd particles (e.g., $w_n = u_{2k+1}$), then we can rewrite Eq. (9) as

$$\rho\ddot{v}_n = [1 + w_{n-1} - v_n]_+^{3/2} - [1 + v_n - w_n]_+^{3/2}, \tag{12}$$
$$\ddot{w}_n = [1 + v_n - w_n]_+^{3/2} - [1 + w_n - v_{n+1}]_+^{3/2}, \tag{13}$$

where we have rescaled time t $\sqrt{A\delta_0}$ and amplitude u $u\delta_0$. We assume that $M > m$, such that the mass ratio $\rho < 1$. Note that these equations under the assumption of small strain,

$$|w_{n-1} - v_n| \ll 1, \quad |w_n - v_n| \ll 1,$$

reduce to the dimer FPUT lattice,

$$\rho\ddot{v}_n = V'(w_n - v_n) - V'(v_n - w_{n-1}), \tag{14}$$
$$\ddot{w}_n = V'(v_{n+1} - w_n) - V'(w_n - v_n), \tag{15}$$

where

$$V'(x) = K_2 x + K_3 x^2 + K_4 x^3, \quad K_2 = \tfrac{3}{2},$$
$$K_3 = -\tfrac{3}{8}, \quad K_4 = -\tfrac{3}{48}.$$

The linearized Eqs. (14) and (15) (i.e., where $K_3 = K_4 = 0$) have solutions of the form $(v_n, w_n)^T = (v^0, w^0)^T e^{i(kn+\ t)}$, where k and are related through the dispersion relation

$$(k)_\pm^2 = K_2\left(1 + \frac{1}{\rho}\right) \pm \sqrt{\left(1 + \frac{1}{\rho}\right)^2 - \frac{4}{\rho}\sin^2\left(\frac{k}{2}\right)}, \tag{16}$$

where the minus and plus signs correspond to the acoustic and optical bands, respectively, of the dispersion relation; see Fig. 1(c). At the wave number $k = \pi$ the upper cutoff frequency of the acoustic band is $_-(\pi) = \sqrt{2K_2}$ and the lower cutoff frequency of the optical band is $_+(\pi) = \sqrt{2K_2/\rho}$. Since $\rho < 1$ there is a band gap of size $_+(\pi) -\ _-(\pi) = \sqrt{\frac{2K_2}{\rho}}(1 - \sqrt{\rho})$. In order to find a rogue wave, we proceed in the same way as in the previous section. Namely, we derive a focusing NLS equation from Eqs. (14) and (15) in order to obtain an approximation that has the Peregrine soliton as the envelope function. This approximation should describe a rogue wave of the dimer granular crystal for small amplitudes. We will make use of numerical simulations to test the role of the nonlinearity stemming from the Hertzian contact. To derive the NLS equation, we use the following ansatz [36]:

$$v_n(t) = \varepsilon(B(X,T) + [A(X,T)E(n,t;0,\ _+(\pi)) + \text{c.c.}]), \tag{17}$$

$$w_n(t) = \varepsilon B(X,T), \tag{18}$$

where

$$E(n,t;k_0,\ _0) = e^{i(k_0 n +\ _0 t)}, \quad X = \varepsilon n, \quad T = \varepsilon^2 t.$$

Here we have already selected the plane wave at the bottom of the optical band to be modulated by the envelope function A, since the notation is less cumbersome than in the general wave-number case. Substitution of this ansatz into Eqs. (14) and (15) leads to the focusing NLS equation at order ε^3:

$$i\partial_T A(X,T) + \nu_2\partial_X^2 A(X,T) + \nu_3 A(X,T)|A(X,T)|^2 = 0,$$
$$\nu_2 = -\frac{''_+(\pi)}{2}, \quad \nu_3 = \frac{K_2^2\ _+(\pi)}{2}(3K_2K_4 - 4K_3). \tag{19}$$

Note that, since $\nu_3 < 0$ and $-\ ''_+(\pi)/2 < 0$, both ν_2 and ν_3 are negative such that Eq. (19) is focusing. The function $B(X,T)$ is defined in terms of $A(X,T)$ via

$$\partial_X B(X,T) = -\frac{4K_3}{K_2}|A(X,T)|^2.$$

Since ν_2 and ν_3 are negative, the Peregrine soliton for Eq. (19) is the same as of Eq. (6) but with the appropriate sign changes:

$$A(X,T) = \sqrt{-\frac{P_0}{\nu_3}}\ \left[1 - \frac{4(1 - 2P_0\, iT)}{1 - \frac{2}{\nu_2}P_0X^2 + 4P_0^2T^2}\right]e^{-iP_0T}. \tag{20}$$

Substituting this expression into Eq. (17) leads to a plane wave that oscillates with temporal frequency $_+(\pi) - \varepsilon^2 P_0$ (and hence lies within the band gap of the spectrum, since $\varepsilon \ll 1$).

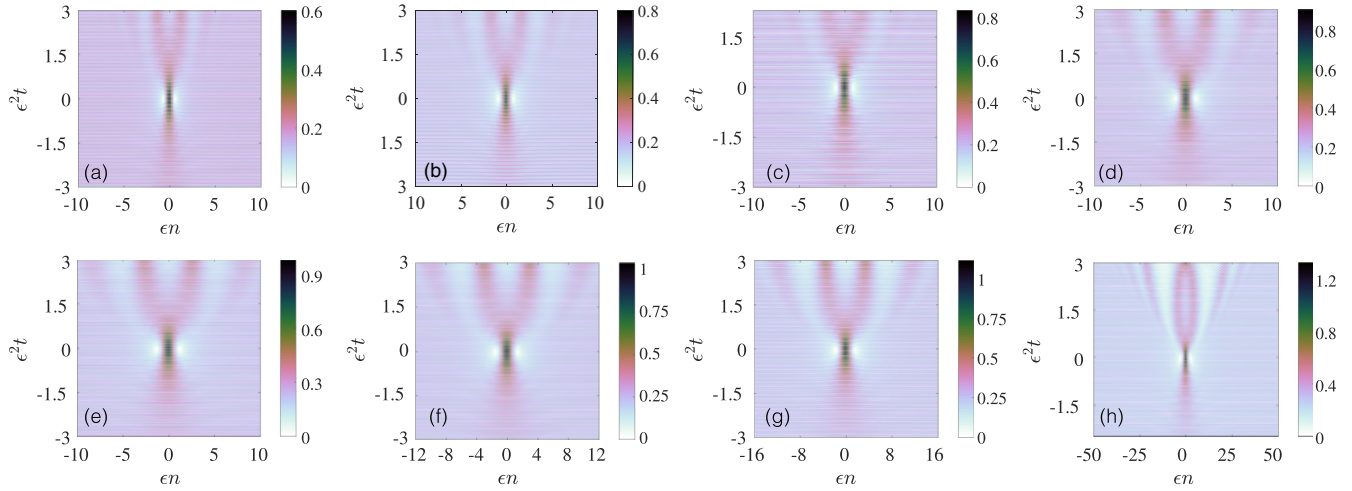

FIG. 4. Simulation of Eq. (9) that is initialized with Eq. (17) and Eq. (18) with A given by Eq. (20) with $P_0 = 1$, $\varepsilon = 0.05$, $X \in [-40, 40]$, and $T \in [-5, 5]$. Color intensity corresponds to the strain $|y_n|$. The values of the mass ratio parameter are (a) $\rho = 0.1$, (b) $\rho = 0.2$, (c) $\rho = 0.3$, (d) $\rho = 0.4$, (e) $\rho = 0.5$, (f) $\rho = 0.6$, (g) $\rho = 0.7$, and (h) $\rho = 0.9$.

B. Peregrine initial data

We conduct a number of simulations of the fully nonlinear dimer crystal model (9) using the ansatz in Eqs. (17) and (18) for various mass ratios. The results are summarized in Fig. 4. For small values of the mass ratio ρ, the dynamics are similar to the monomer FPU chain studied above. There is the appearance of a large amplitude peak, seemingly out of nowhere, but then rather than disappearing "without a trace," as the NLS Peregrine soliton predicts, the large amplitude portion of the wave breaks into smaller, but still large relative to the background, waves (compare Fig. 4 and Fig. 2). The same feature persists for larger mass ratios, however, the secondary pulses become broader. This is part of the manifestation of the modulational instability of the corresponding background. For sufficiently large mass ratios ρ, more waves seem to emerge as a result of the instability, and the timescale of their interaction appears to be shorter.

We have also observed a substantial sensitivity to boundary conditions and a rapid propagation of the resulting excitations, reflecting from the boundary towards the core of the Peregrine structure. It is relevant to note here that for uncompressed granular crystals, solitary waves are found to exist at special mass ratios (the so-called antiresonances), and severe wave attenuation occurs at other special mass ratios (the so-called resonances) [42–45]. It would be particularly interesting to explore whether such phenomena have an analog in the case of precompressed diatomic granular crystals and whether they have any implications towards the formation of the Peregrine solitons. Future studies concerning resonances and antiresonances of precompressed diatomic granular chains would therefore not only be interesting in their own right, but might also help explain the observed deviations from granular crystal dynamics and the NLS predictions.

C. Gaussian initial data

We now complement the results obtained from Gaussian initial data in the monomer FPUT model with the case of the diatomic granular crystal. We consider initial data for the envelope function $A(X, T)$ of the form

$$A(X, T = 0) = \alpha \exp\left(\frac{-\beta X^2}{2\sigma^2}\right), \tag{21}$$

where the scaling parameters $\alpha = \sqrt{1/v_3}$ and $\beta = 2v_2$ are chosen to make the evolution consistent with the results obtained in the monomer FPUT case (since the values of the NLS coefficients v_2 and v_3 are different in the NLS equation derived for the dimer granular crystal).

In Fig. 5 results for simulations for the parameter values $\sigma \in \{10.5, 2.5, 1.3\}$, $\varepsilon = 0.05$, and $\rho \in \{0.6, 0.4, 0.2\}$ are shown. The results are similar to what was obtained in the FPUT model [compare Figs. 3(e)–3(h) and Fig. 5]. An interesting observation is that as the mass ratio ρ varies, the transition between the different types of behavior (as the width of the initial Gaussian changes) also changes. For example, the breathing pattern that is observed for $\rho = 0.6$ and $\sigma = 2.5$ occurs when $\rho = 0.4$ and $\sigma = 1.3$. Similarly the phenomenology of $\rho = 0.4$ for $\sigma = 2.5$ seems most strongly reminiscent of that of $\rho = 0.2$ for $\sigma = 1.3$ etc. Thus the transition has been effectively shifted. Admittedly, in this dimer setting, one can observe the emerging formation of more "permanent" structures; see, e.g., along the diagonal of Fig. 5, e.g., past $\varepsilon^2 t = 10$. Nevertheless, the initial stage of space-time localization, resulting from the focusing of the Gaussian initial data for sufficiently large σ suggests the presence of a structure reminiscent of the Peregrine solitary wave. Subsequently for smaller σ (see, e.g., the superdiagonal of Fig. 5) one obtains a breathing pattern and eventually (see the top right panel of the figure) a permanent, spatially localized solitary wave form.

D. Extreme events resulting from modulation instability

Our analysis involving the NLS equation obtained via a long wavelength approximation offered us insight to the formation of rogue waves in the model describing dimer granular crystals. However, the size of the lattice considered thus far has been too large for a realistic experimental setup ($N = 2001$ particles). Moreover, within current experimental capabilities, it is not

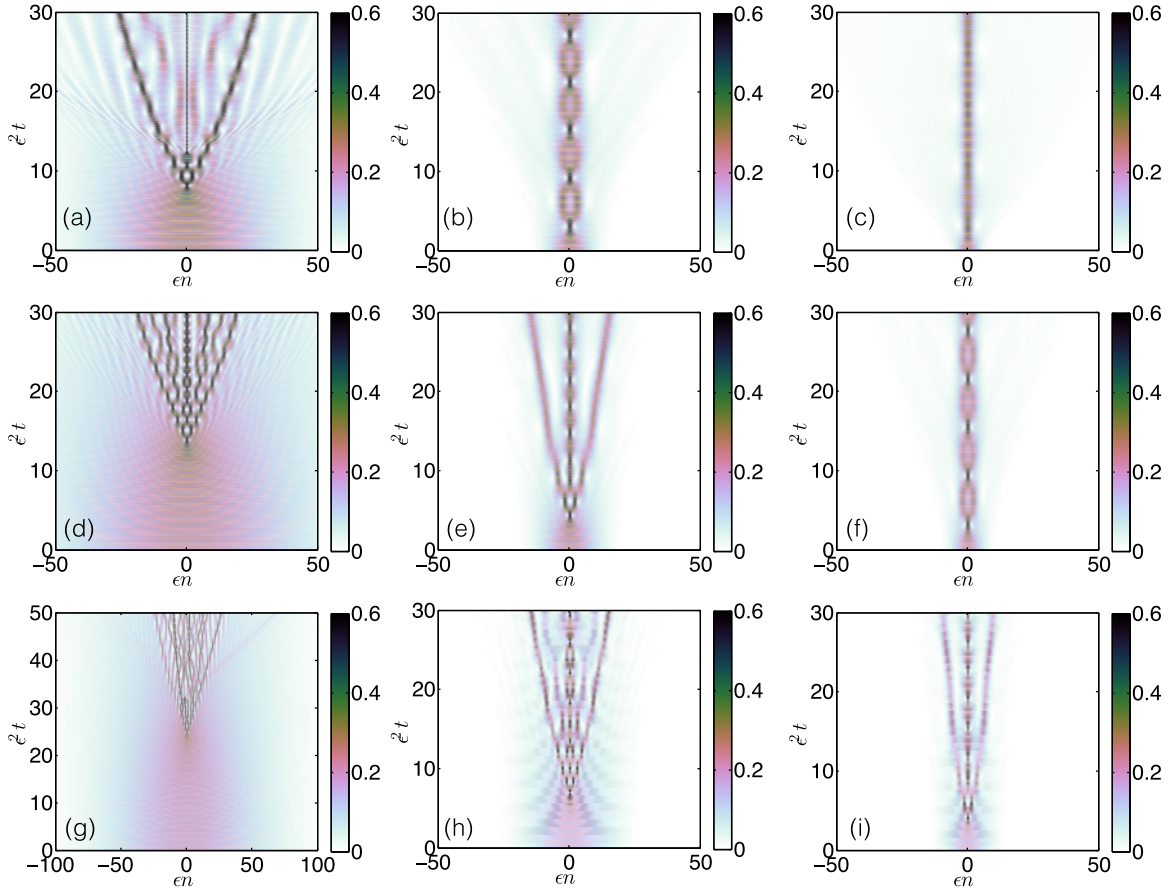

FIG. 5. Simulation of Eq. (9) that is initialized with Eq. (17) and Eq. (18) with A given by Eq. (21) with the following parameters: The top row has $\rho = 0.6$ and $\sigma = 10.5$ (a), $\sigma = 2.5$ (b), and $\sigma = 1.3$ (c). The middle row has $\rho = 0.4$ and $\sigma = 10.5$ (d), $\sigma = 2.5$ (e), and $\sigma = 1.3$ (f). The bottom row has $\rho = 0.2$ and $\sigma = 10.5$ (g), $\sigma = 2.5$ (h), and $\sigma = 1.3$ (i).

possible to initiate the positions and velocities of each particle in the chain. Experimentalists have the capability of striking the chain [26], actuating one or more of the boundaries [46], and controlling the precompression level while actuating the chain [41]. Thus, we now consider a situation where an extreme event can be induced in a granular chain through modification of the boundary only. In the NLS equation, it is well known that plane waves at the edge of the linear spectrum evolving through the nonlinear equations of motion can exhibit a modulation instability (MI) [4]. The consequence of the MI relies heavily on the initial condition, and the result could be the formation of a soliton, a two-soliton (or more generally an N-soliton [47]), a Peregrine soliton (or more generally multiple such as in the gradient catastrophe scenario of Ref. [38]), or different kinds of states, such as the (space-periodic) Akhmediev breather or (time-periodic) Kuznetsov-Ma soliton, or cnoidal waves as in the recent studies of Ref. [48]. In the case of the NLS equation, identifying which structure results from the MI is possible since exact solutions for the soliton, Peregrine soliton, Akhmediev breather and Kuznetsov-Ma solitons are available. In the case of the dimer granular chain, no such formulas exist, to the best of our knowledge. Thus, motivated by the well-understood notion of MI in models such as the NLS equation, we will excite a plane wave at the edge of the linear spectrum (in this case the bottom of the optical band) and observe how MI will affect the plane wave. Our goal is to identify an extreme event, although given the complex nature of the resulting phenomenon, what particular structural name is most appropriate to assign to this event (e.g., discrete breather or Peregrine soliton or some other structure) will be left as an open subject for further consideration. The model in dimensional form is

$$M_n\ddot{u}_n = A[\delta_0 + u_{n-1} - u_n]_+^{3/2} - A[\delta_0 + u_n - u_{n+1}]_+^{3/2} - M_n\dot{u}_n/\tau, \tag{22}$$

where $A = 7.24 \times 10^9\ \mathrm{kg\,m^{-5/2}\,s^{-2}}$, $\delta_0 = 0.2813\ \mu$m, $M_n = 9.7$ g for n even, and $M_n = 28.8$ g for n odd. This corresponds to a mass ratio of $\rho = 0.33$. These parameter values are consistent with experimental setups of granular chains [41,46]. The term $-M_n\dot{u}_n/\tau$ is a simple description of the damping of the system [41]. We first consider the undamped case $\tau \quad \infty$. To excite the plane wave we simply actuate the boundaries [$u_{\mathrm{left}} = u_{\mathrm{right}} = a\cos(2\pi f t)$] of a chain of length $N = 41$ at the appropriate frequency ($f = 8.9$ kHz in the example used) with a low amplitude ($a = 0.001\ \mu$m) until the corresponding mode is formed (until $t = 0.01$ s); see, for example, Fig. 6(a). Since the actuation amplitude is low, the response is essentially linear ($\max_n |u_n - u_{n+1}|/\delta_0 = 0.06$). After the linear mode has formed (propagating through the chain), we want the nonlinearity to start having an (instability-inducing) effect on the mode, so we decrease the

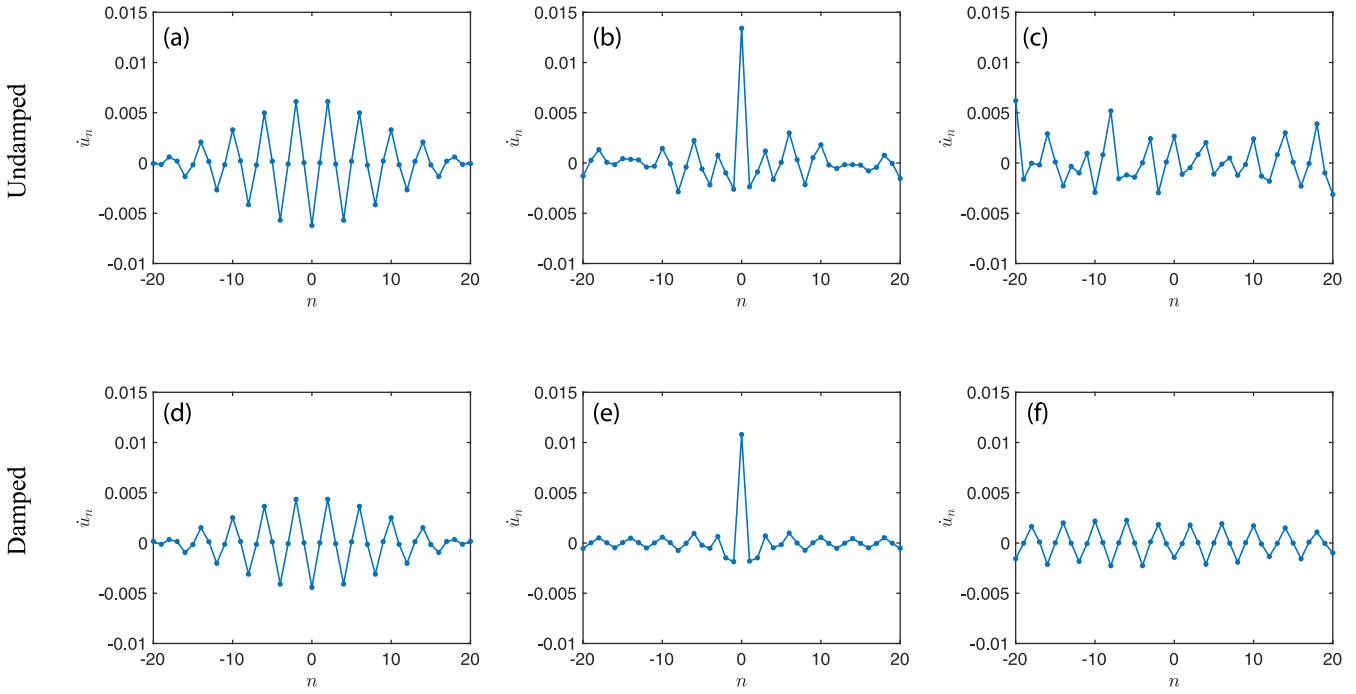

FIG. 6. Spatial distribution of velocity profiles is shown at (a) and (d) $t = 0.01$ s, (b) $t = 0.104$ s, (c) and (f) $t = 0.2$ s, and (e) $t = 0.106$ s. (a) Velocity of solution after exciting an at rest dimer chain at the boundaries at a frequency at the bottom of the lower optical band. (b) After the precompression is decreased by a factor of 7, the system behaves nonlinearly, causing the onset of MI. This results in the spatial localization of the solution. (c) The localization is not persistent. (d–f) Same as panels (a)–(c) but in a damped system with $\tau = 70$ ms.

strength of the precompression by a factor of 7 such that there will be a nonlinear response ($\max_n |u_n - u_{n+1}|/\delta_0 = 0.42$). The MI causes the mode to spontaneously localize; see Fig. 6(b). This is a phenomenology rather reminiscent of the the discrete breather formation reported in Ref. [46]. That being said, we also find that this localization does not persist, as the structure becomes delocalized; see Fig. 6(c). A space-time contour plot of this process is shown in Fig. 7(a). We performed the same numerical experiment described above in the presence of a dashpot damping term $-M_n\dot{u}_n/\tau$, where $\tau = 70$ ms describes the damping strength; see Figs. 6(d)–6(f) and Fig. 7(b). In this case, the phenomenology presents an emerging form of space-time localization structurally rather reminiscent of the Peregrine soliton, although once again the temporal localization may well be due to the presence of dissipation rather than the inherent (NLS-based) Hamiltonian dynamics. We note in passing here that $\tau = 70$ ms represents very low damping (for example, in Ref. [41] the damping constant was $\tau = 5$ ms). In our simulations, extreme events were not detectable for systems with damping constants $\tau < 70$ ms. This suggests that the quantitative characteristics of damping could play a significant role in the potential emergence of extreme events in experimental systems, and that the ability to limit damping would be crucial in observing the relevant phenomenology.

IV. DISCUSSION AND FUTURE DIRECTIONS

In the present study, we have definitively illustrated the potential of phononic lattices to support rogue wave structures.

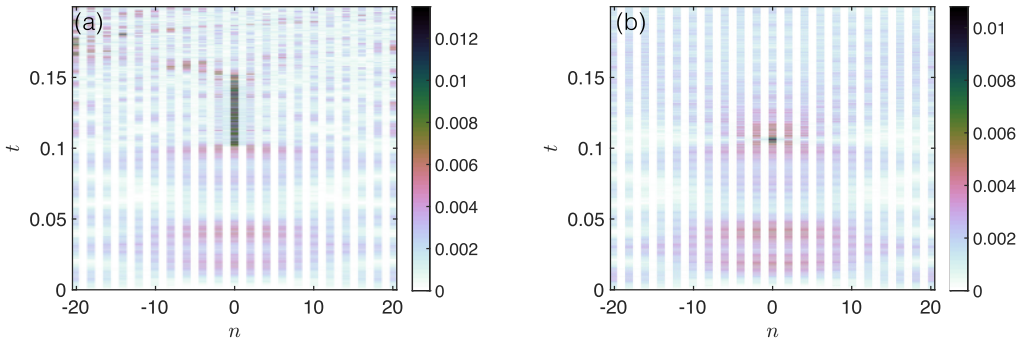

FIG. 7. (a) Space-time contour plot corresponding to panels (a)–(c) of Fig. 6, which shows the onset of MI. (b) Space-time contour plot corresponding to panels (d)–(f) of Fig. 6.

Our preliminary considerations focused on the FPUT lattice as a prototypical example where rogue waves could be excited by using the Peregrine soliton solution of the derived NLS equation as initial data. For sufficiently wide Gaussians, we also found rogue-wave patterns in line with the universality of the gradient catastrophe mechanism suggested by Ref. [38]. However, for Peregrine and Gaussian initial data, the formation of the large amplitude structures led eventually to deviations in the FPUT dynamics from the expected predictions of the NLS approximation. While part of the observed discrepancies may be attributed to boundary effects, the predominant reason for this phenomenology is the presence of the modulational instability for the background on top of which the Peregrine structure is formed. We also considered a diatomic granular crystal to demonstrate that rogue wave dynamics is possible in a system that is highly accessible in experiments in a space-time resolved way [30]. A key challenge in that regard concerns the large scales considered in this paper (where the NLS approximation is valid) leading to large lattices. However, it may be interesting to try relevant ideas in smaller lattices; some studies have considered lattices as large as $N = 81$ nodes [46] or even $N = 188$ nodes in Ref. [49]. While this paper establishes important first steps for the realization of phononic rogue waves, future theoretical studies should consider further steps in some of these directions; another important one involves the suitable initialization with Peregrine-like initial data, as these lattices permit considerable control, e.g., over driving the boundaries, but are less amenable to a distributed initialization over the entire chain. Such topics are presently under consideration and will be reported in future publications.

ACKNOWLEDGMENTS

P.G.K. gratefully acknowledges discussions with S. Sen at an early stage of this work. We give special thanks to Ariel Gonzales and Anam Shah (funded by the Bowdoin Science Experience work-study program) for help with simulations and data management. This material is based upon work supported by the National Science Foundation under Grant No. DMS-1615037 (C.C.). P.G.K. gratefully acknowledges support from the US-AFOSR under Grant No. FA9550-17-1-0114. P.G.K. acknowledges that this work was made possible by NPRP Grant No. 8-764-1-160 from Qatar National Research Fund (a member of Qatar Foundation). The findings achieved herein are solely the responsibility of the authors.

[1] E. Pelinovsky and C. Kharif, editors, *Extreme Ocean Waves* (Springer, New York, 2008).
[2] C. Kharif, E. Pelinovsky, and A. Slunyaev, *Rogue Waves in the Ocean* (Springer, New York, 2009).
[3] A. R. Osborne, *Nonlinear Ocean Waves and the Inverse Scattering Transform* (Academic Press, Amsterdam, 2010).
[4] C. Sulem and P.-L. Sulem, *The Nonlinear Schrödinger Equation: Self-Focusing and Wave Collapse* (Springer, New York, 1999).
[5] D. H. Peregrine, J. Austral. Math. Soc. B **25**, 16 (1983).
[6] D. R. Solli, C. Ropers, P. Koonath, and B. Jalali, Nature (London) **450**, 1054 (2007).
[7] B. Kibler *et al.*, Nat. Phys. **6**, 790 (2010).
[8] B. Kibler *et al.*, Sci. Rep. **2**, 463 (2012).
[9] J. M. Dudley, F. Dias, M. Erkintalo, and G. Genty, Nat. Photon. **8**, 755 (2014).
[10] B. Frisquet *et al.*, Sci. Rep. **6**, 20785 (2016).
[11] C. Lecaplain, Ph. Grelu, J. M. Soto-Crespo, and N. Akhmediev, Phys. Rev. Lett. **108**, 233901 (2012).
[12] A. N. Ganshin, V. B. Efimov, G. V. Kolmakov, L. P. Mezhov-Deglin, and P. V. E. McClintock, Phys. Rev. Lett. **101**, 065303 (2008).
[13] A. Chabchoub, N. P. Hoffmann, and N. Akhmediev, Phys. Rev. Lett. **106**, 204502 (2011).
[14] A. Chabchoub, N. Hoffmann, M. Onorato, and N. Akhmediev, Phys. Rev. X **2**, 011015 (2012).
[15] A. Chabchoub and M. Fink, Phys. Rev. Lett. **112**, 124101 (2014).
[16] H. Xia, T. Maimbourg, H. Punzmann, and M. Shats, Phys. Rev. Lett. **109**, 114502 (2012).
[17] M. Shats, H. Punzmann, and H. Xia, Phys. Rev. Lett. **104**, 104503 (2010).
[18] H. Bailung, S. K. Sharma, and Y. Nakamura, Phys. Rev. Lett. **107**, 255005 (2011).
[19] E. G. Charalampidis, J. Cuevas-Maraver, D. J. Frantzeskakis, and P. G. Kevrekidis, Rom. Rep. Phys. **70**, 504 (2018).
[20] Y. Shen, P. G. Kevrekidis, G. P. Veldes, D. J. Frantzeskakis, D. DiMarzio, X. Lan, and V. Radisic, Phys. Rev. E **95**, 032223 (2017).
[21] N. Akhmediev and A. Ankiewicz, Phys. Rev. E **83**, 046603 (2011).
[22] D. Han, M. Westley, and S. Sen, Phys. Rev. E **90**, 032904 (2014).
[23] E. Fermi, J. Pasta, and S. Ulam, Studies in nonlinear problems, I. Los Alamos report, LA 1940 (1955).
[24] G. Gallavotti, *The Fermi-Pasta-Ulam Problem: A Status Report* (Springer, Berlin, 2008).
[25] P. G. Kevrekidis, IMA J. Appl. Math. **76**, 389 (2011).
[26] V. F. Nesterenko, *Dynamics of Heterogeneous Materials* (Springer, New York, 2001).
[27] S. Sen, J. Hong, J. Bang, E. Avalos, and R. Doney, Phys. Rep. **462**, 21 (2008).
[28] G. Theocharis, N. Boechler, and C. Daraio, in *Acoustic Metamaterials and Phononic Crystals* (Springer, Berlin, 2013), pp. 217–251.
[29] A. F. Vakakis, in *Wave Propagation in Linear and Nonlinear Periodic Media*, International Center for Mechanical Sciences (CISM) Courses and Lectures (Springer, Berlin, 2012), p. 257.
[30] C. Chong, M. A. Porter, P. G. Kevrekidis, and C. Daraio, J. Phys.: Condens. Matter **29**, 413003 (2017).
[31] M. A. Porter, P. G. Kevrekidis, and C. Daraio, Phys. Today **68**, 44 (2015).
[32] Y. Starosvetsky, K. Jayaprakash, M. A. Hasan, and A. Vakakis, *Dynamics and Acoustics of Ordered Granular Media* (World Scientific, Singapore, 2017).
[33] A. Rosas and K. Lindenberg, Phys. Rep. **735**, 1 (2018).
[34] G. Schneider, Appl. Anal. **89**, 1523 (2010).
[35] G. Huang, Z.-P. Shi, and Z. Xu, Phys. Rev. B **47**, 14561 (1993).

[36] G. Huang and B. Hu, Phys. Rev. B **57**, 5746 (1998).
[37] K. Hammani, B. Kibler, C. Finot, P. Morin, J. Fatome, J. M. Dudley, and G. Millot, Opt. Lett. **36**, 112 (2011).
[38] M. Bertola and A. Tovbis, Commun. Pure Appl. Math. **66**, 678 (2013).
[39] A. Tikan, C. Billet, G. El, A. Tovbis, M. Bertola, T. Sylvestre, F. Gustave, S. Randoux, G. Genty, P. Suret, and J. M. Dudley, Phys. Rev. Lett. **119**, 033901 (2017).
[40] C. Chong, P. G. Kevrekidis, G. Theocharis, and C. Daraio, Phys. Rev. E **87**, 042202 (2013).
[41] C. Chong, F. Li, J. Yang, M. O. Williams, I. G. Kevrekidis, P. G. Kevrekidis, and C. Daraio, Phys. Rev. E **89**, 032924 (2014).
[42] K. R. Jayaprakash, Y. Starosvetsky, and A. F. Vakakis, Phys. Rev. E **83**, 036606 (2011).
[43] K. R. Jayaprakash, Y. Starosvetsky, A. F. Vakakis, and O. V. Gendelman, J. Nonlinear Sci. **23**, 363 (2013).
[44] E. Kim, R. Chaunsali, H. Xu, J. Jaworski, J. Yang, P. G. Kevrekidis, and A. F. Vakakis, Phys. Rev. E **92**, 062201 (2015).
[45] Y. Zhang, D. Pozharskiy, D. M. McFarland, P. G. Kevrekidis, I. G. Kevrekidis, and A. F. Vakakis, Exp. Mech. **57**, 505 (2017).
[46] N. Boechler, G. Theocharis, S. Job, P. G. Kevrekidis, M. A. Porter, and C. Daraio, Phys. Rev. Lett. **104**, 244302 (2010).
[47] J. Satsuma and N. Yajima, Prog. Theor. Phys. Suppl. **55**, 284 (1974).
[48] G. Biondini and D. Mantzavinos, Phys. Rev. Lett. **116**, 043902 (2016); see also: G. Biondini, S. Li, and D. Mantzavinos, Phys. Rev. E **94**, 060201(R) (2016).
[49] R. Carretero-González, D. Khatri, M. A. Porter, P. G. Kevrekidis, and C. Daraio, Phys. Rev. Lett. **102**, 024102 (2009).